

ORIGINAL ARTICLE

Open Access



Flexible Scanning Method by Integrating Laser Line Sensors with Articulated Arm Coordinate Measuring Machines

Zexiao Xie^{*} , Ping Yu, Hanlei Gong, Shukai Chi and Xiang Gao

Abstract

Measuring and reconstructing the shape of workpieces have been considered as a fundamental step in both reverse engineering and product quality control. Owing to increasing structural complexity of recent products, measurements from multiple directions are typically required in current scanning techniques. Specifically, the plane structured light can be applied to measure one area of a part at a time, with an additional algorithm required to merge the collected data of each area. Alternatively, the line structured light sensor integrated on CNC machines or CMMs could also realize multi-view measurement. However, the system needs to be repeatedly calibrated at each new direction. This paper presents a flexible scanning method by integrating laser line sensors with articulated arm coordinate measuring machines (AACMM). Since the output of the laser line sensor is 2D raw data in the laser plane, our system model introduces an explicit transformation from the 2D sensor coordinate frame to the 3D base coordinate frame of the AACMM (i.e., the translation and rotation of the 2D sensor coordinate in the sixth coordinate system of AACMM). To solve the model, the “conjugate pairs” are proposed and identified by measuring a fixed point (e.g., a sphere center). Moreover, a search algorithm is adopted to find the optimal solution, which noticeably boosts the model accuracy. The experimental results show that the error of the system is about 0.2 mm, which is caused by the error of the AACMM, the sensor error and the calibration error. By measuring a complicated part, the proposed system is proved to be flexible and facilitate, with the ability to measure a part expediently from any necessary direction. Furthermore, the proposed calibration method can also be used for robot hand-eye relationship calibration.

Keywords: Reverse engineering, Laser line sensors, Articulated arm coordinate measuring machines, Conjugate pairs

1 Introduction

With the development of modern manufacturing industry, reverse engineering has been playing an increasingly important role in the fields of aviation, automobile and house appliance [1, 2]. The products in these fields are becoming more and more complex and irregular. If a part could be measured accurately and completely, its CAD model can be reconstructed correctly and efficiently. In the field of manufacturing, more and more product geometric dimensions also need to be measured quickly and

accurately [3, 4]. To meet these requirements, visual-based measurement methods, such as laser beam probes and structured-light laser sensors have been widely used benefited from their attributes of non-contact, high-speed, and high-accuracy, etc. [5]. Laser beam sensors can be considered as a 1D sensor that outputs a distance value from the zero reading point. When the laser beam sensor is used for scanning, it is usually installed on the CMM. The transformation relationship from the 1D coordinate on the laser beam to the 3D coordinate of the CMM should be determined [6].

The structured light mainly consists of two categories of the line structured light and the plane structured light [7]. The plane structured light is a portable and efficient

*Correspondence: xiezexiao@ouc.edu.cn

College of Engineering, Ocean University of China, Qingdao 266100, China

measurement approach. It can measure an area of a part at a time. Specifically, several areas on a part need to be plotted out before independent measurements of each area, and the collected data on different areas can then be merged using special algorithm [8, 9] or CAD systems, such as Rapidform and Polyworks. Compared with plane structured light, line structured light has high robustness to dark objects and highly reflective objects because of its good monochromaticity and high brightness [10].

In the line structure light 3D measurement technique, the measurement accuracy mainly depends on the laser light plane calibration. The main issue is to identify the relationship between the light plane and CCD array plane. To address this issue, a series of light plane calibration methods with different targets have been developed. Dependent on the requirements, 3D targets [11, 12], 2D targets [13–15] and 1D targets [16] could be applied to a variety of scenes.

However, the line structured light can only acquire one single line for each measurement, makes it difficult to obtain the full-view shape of the object through one-time measurement. It can realize non-contact 3D scanning only when it is integrated into CMMs or CNC machine tools [17]. The data collected by line structured light sensors, which is expressed in 2D format must be transformed into 3D format in world coordinate system. Xie et al. [18] proposed a five-axis system in which a laser line sensor is mounted on a PH10 rotary head and the PH10 is mounted on the Z-axis of a CMM. He mainly studied the relationship between the 2D coordinate system in the light plane and the CMM 3D world coordinate system, that is, the extrinsic parameters of structured light. Santolaria et al. [19] and Xie et al. [20] proposed a method for simultaneously calibrating intrinsic and extrinsic parameters of structured-light sensors respectively.

In addition to being mounted on a 3D mechanism, structured-light sensors can be positioned by other methods. In Ref. [21], a laser tracker and an industrial robot are used to provide position for structured-light sensor to obtain 3D data, which can achieve high position accuracy by using a highcost laser tracker. In Ref. [22], a turntable is used to provide rotation coordinates. This method is relatively flexible, but it can only measure small rotating objects. Optical positioning is a new method by using cameras, but the positioning accuracy is not easy to be controlled [23].

In recent years, handheld laser scanning technology has been developed rapidly and been widely used. Its main feature is that it can flexibly change the angle according to the characteristics of the object and measure all areas on the object. Moreover, it is not limited by the measurement range and can measure large objects [24]. However, before measurement, a large number of circular mark

points must be pasted on the object in order to locate the measurement system. Therefore, this method is not very convenient in real-time measurement.

To overcome the bottleneck of measuring the parts with complex structure and features completely and efficiently, this paper presents a flexible scanning system by integrating a laser line sensor with an AACMM, as shown in Figure 1. The system can measure complicated parts by manually controlling the arms to change the orientation of the laser sensor, therefore accessing any area on the part.

In this study, the relationship between laser sensor and AACMM is similar to the hand-eye relationship of robot, which can be determined based on the position relationship between the end joint of the robot and the vision systems, including the binocular vision and monocular vision. In this case, a target is usually used as a calibration object, so that the vision system can observe the target and obtain the calibration point under the fixed target position, as a known condition to solve the hand-eye relationship. Yin et al. [25] proposed a method to calibrate the hand-eye relationship using a standard sphere. The feasibility of this method is that the motion of the robot can be controlled and the laser plane can be controlled to pass through the sphere center. Sharifzadeh et al. [26] calibrated the hand-eye relationship using a flat plate. It is also because the motion of the robot is controllable, the structured light projected onto the flat plate shows a circular pattern. Qin et al. [27] calculated the sensor rotational errors reversely from the data dislocation originating from the sensor without calibration, and then calibrated the sensor by mechanical adjustment and

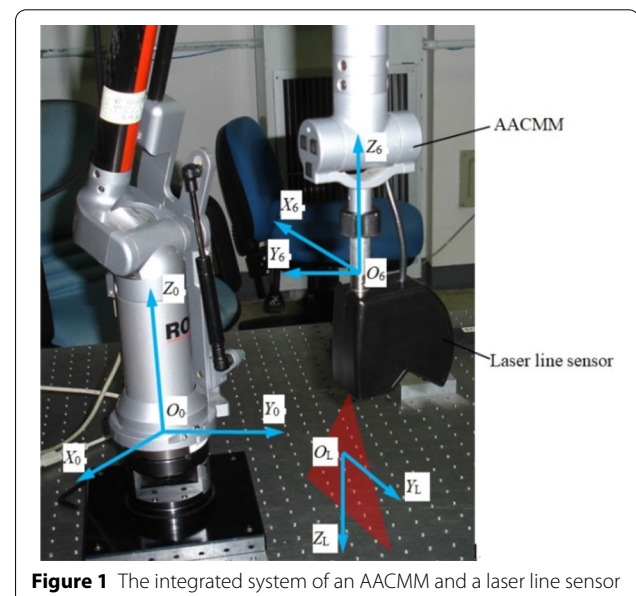


Figure 1 The integrated system of an AACMM and a laser line sensor

numerical compensation. In this method, the stitching of data depends on objects with special structure such as honeycomb cores. Yu et al. [28] calibrated the light plane of the line structured light using binocular cameras which simplifies the calibration process and improves the 3D measurement accuracy. When the calibration is completed, the camera 2 is removed. This method is reasonable in principle, but it is inconvenient in practical use.

2 System Modelling

An articulated arm CMM (AACMM) usually has six or seven rotation axes to access a point in 3D space from almost any direction. Figure 2 shows a simplified model of a six-axis articulated arm CMM. In this model, $O_0X_0Y_0Z_0, \dots, O_5X_5Y_5Z_5$ are the six coordinate frames located on each rotation axis, with $O_0X_0Y_0Z_0$ the base coordinate frame and $O_6X_6Y_6Z_6$ the coordinate frame of a touch probe. In Figure 1, the touch probe originally mounted on AACMM is replaced by a laser line sensor, while the definition of touch probe coordinates $O_6X_6Y_6Z_6$ still applies: O_6 is located at the position of the tip of the touch probe; Y_6 is parallel to the last axis (Z_5) of the arm; Z_6 points towards the inwards direction along the touch probe; the remaining direction of X_6 can be determined by right-hand rule.

For a commercial AACMM, the transformations from $O_6X_6Y_6Z_6$ to $O_0X_0Y_0Z_0$ can be performed based on SDK information provide by manufacturers. In another word, it is possible to directly obtain the coordinate of

the touch probe O_6 and the direction vector of X_6 , Y_6 and Z_6 in the base coordinate frame $O_0X_0Y_0Z_0$. After calibration of intrinsic parameters of the laser sensor, a 2D coordinate frame $O_LY_LZ_L$ in the laser plane can be established, according to Figures 1 and 2. When the laser sensor is employed for scanning, 2D raw data points in the frame $O_LY_LZ_L$ are recorded. Since the transformation from $O_6X_6Y_6Z_6$ to $O_0X_0Y_0Z_0$ is known, once the transformation from $O_LY_LZ_L$ to $O_6X_6Y_6Z_6$ is determined, the scanned 2D data point can be then transformed into 3D data point in the base coordinate frame $O_0X_0Y_0Z_0$.

The articulated arm CMM adopted in this paper is Romer 2028, which has six axes. The communications between the AACMM and the computer are fulfilled through a USB interface. The computer can directly read twelve parameters from the AACMM. The sequence of the parameters reading from Romer 2028 is $(r_1 \ r_4 \ r_7)$, $(r_2 \ r_5 \ r_8)$, and $(r_3 \ r_6 \ r_9)$, $(q_x \ q_y \ q_z)$, corresponding to the direction vectors of X_6 , Y_6 , Z_6 , and the coordinate of O_6 in the base coordinate frame $O_0X_0Y_0Z_0$. The matrix form is

$$T_0^6 = \begin{bmatrix} r_1 & r_2 & r_3 & q_x \\ r_4 & r_5 & r_6 & q_y \\ r_7 & r_8 & r_9 & q_z \\ 0 & 0 & 0 & 1 \end{bmatrix}. \quad (1)$$

Eq. (1) is the transformation from $O_6X_6Y_6Z_6$ to $O_0X_0Y_0Z_0$.

The transformation from $O_LY_LZ_L$ to $O_6X_6Y_6Z_6$ is a 2D to 3D transformation, which can be established as

$$T_6^L = \begin{bmatrix} l_y & l_z & t_x \\ m_y & m_z & t_y \\ n_y & n_z & t_z \\ 0 & 0 & 1 \end{bmatrix}, \quad (2)$$

where $(l_y \ m_y \ n_y)$ is the direction vector of Y_L , $(l_z \ m_z \ n_z)$ is the direction vector of Z_L , $(t_x \ t_y \ t_z)$ is the translation of $O_LY_LZ_L$ in $O_6X_6Y_6Z_6$. All parameters in Eq. (2) are unknown.

According to Eqs. (1) and (2), the system model is established to transform the 2D data point in $O_LY_LZ_L$ into 3D data point in $O_0X_0Y_0Z_0$ by

$$P_0 = T_0^6 T_6^L P_L, \quad (3)$$

or

$$\begin{bmatrix} x_0 \\ y_0 \\ z_0 \\ 1 \end{bmatrix} = \begin{bmatrix} r_1 & r_4 & r_7 & q_x \\ r_2 & r_5 & r_8 & q_y \\ r_3 & r_6 & r_9 & q_z \\ 0 & 0 & 0 & 1 \end{bmatrix} \begin{bmatrix} l_y & l_z & t_x \\ m_y & m_z & t_y \\ n_y & n_z & t_z \\ 0 & 0 & 1 \end{bmatrix} \begin{bmatrix} y_L \\ z_L \\ 1 \end{bmatrix}, \quad (4)$$

where P_L is the coordinate of a point in $O_LY_LZ_L$, and P_0 is the coordinate of the same point in $O_0X_0Y_0Z_0$.

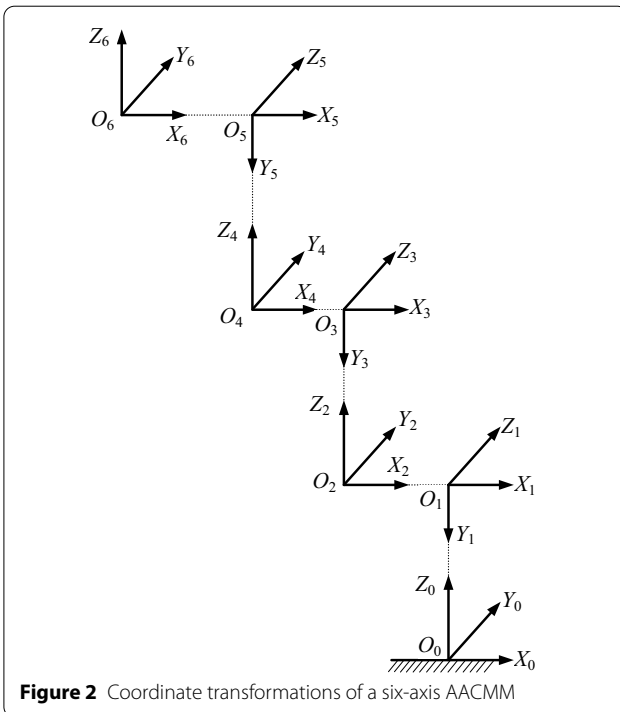


Figure 2 Coordinate transformations of a six-axis AACMM

3 Calibration of T_6^L

In Eqs. (3) and (4), the parameters in T_0^6 are directly read from the articulated arm CMM, while the parameters in T_6^L are unknown and need to be calibrated. (y_L, z_L) is given by the laser line sensor, which is the coordinate of a point in $O_L Y_L Z_L$, and (x_0, y_0, z_0) is the coordinate of the same point in $O_0 X_0 Y_0 Z_0$. If T_0^6 , T_6^L and (y_L, z_L) are all determined, (x_0, y_0, z_0) can be worked out.

T_6^L and P_0 are the unknown parameters in Eq. (3). If (x_0, y_0, z_0) is always the same point during the process of calibration of T_6^L , the total number of unknown parameters in Eq. (4) is twelve, otherwise this number of unknown parameters in Eq. (4) is uncertain.

The calibration process is to build some sets of T_0^6 and (y_L, z_L) , which are then substituted into Eq. (4) to establish an equations set that further solves T_6^L and (x_0, y_0, z_0) . To ensure that (x_0, y_0, z_0) does not change with the alternation of T_0^6 and (y_L, z_L) , a fixed point in $O_0 X_0 Y_0 Z_0$ should be measured. In this paper when a fixed point is measured using the sensor, the measured (y_L, z_L) in $O_L Y_L Z_L$ and T_0^6 are defined as a “conjugate pair”. In principle, four conjugate pairs are sufficient to solve the twelve unknown parameters. On the other hand, as $O_L Y_L Z_L$ is an orthogonal coordinate frame, three constraints can be picked up from Eq. (4):

$$\begin{cases} l_y^2 + m_y^2 + n_y^2 = 1, \\ l_z^2 + m_z^2 + n_z^2 = 1, \\ l_y l_z + m_y m_z + n_y n_z = 0. \end{cases} \quad (5)$$

Because of the nonlinearity of Eq. (5), using only these conditions to solve twelve unknown parameters will give a non-stable solution, and the accuracy of the solution can be affected seriously by the errors of conjugate pairs. In order to avoid these problems, more conjugate pairs should be established. Therefore, the calculation of T_6^L becomes a non-linear constrained least-square optimization problem.

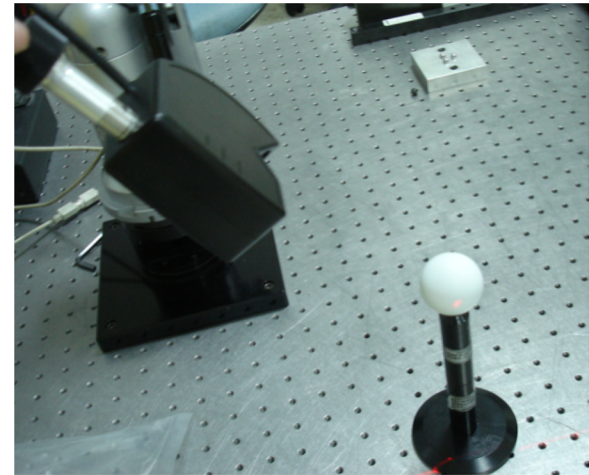
$$F = \sum_{i=1}^n |P_{0i} - T_0^6 T_6^L P_{Li}|^2. \quad (6)$$

4 Conjugate Pairs Identification

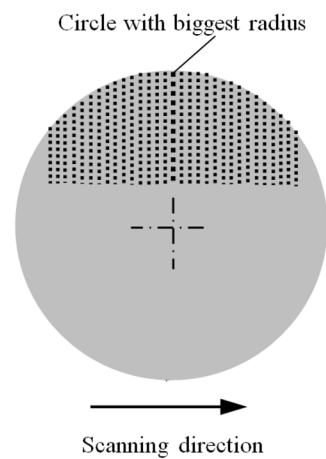
In the calibration process, how to get “conjugate pairs” is the key problem. To solve this problem, a fixed point is measured several times by the sensor at different coordinates (y_L, z_L) from different directions. In practice, it is difficult to project the laser stripe onto a fixed point by manually controlling the sensor.

Usually, the center coordinate of a sphere can always be found by sphere fitting using the measured points

on the surface of the sphere. Apart from sphere fitting, the center of the sphere can also be obtained by circle fitting if the laser plane passes through the sphere center. In this paper, a sphere is scanned with many lines captured as demonstrated in Figure 3, and the 2D data points on each line are applied to fit a circle. If the laser lines are dense enough, the circle with biggest radius would be corresponding to the position of the AACMM, where the laser plane passes through the center of the sphere. Fixed-point measurements by the laser line sensor can be therefore achieved. At the meantime, T_0^6 (AACMM position) and the center of the sphere (y_L, z_L) , i.e., a “conjugate pair” is obtained.



(a)



(b)

Figure 3 (a) Scanning a sphere and fitting circle using the 2D points on the laser line, (b) Center of the circle with biggest radius corresponding to the center of the sphere

After calibration, the measurement accuracy should be consistent with any AACMM coordinate and sensor value within their working ranges. Therefore, in the process of calibration each axis of the arm should be rotated within its range as large as possible. The laser plane intersects the sphere with different working region as shown in Figure 4. By substituting these conjugate pairs into Eq. (6), the twelve unknown parameters can be worked out.

It is important to note that the center of the sphere

in T_6^L can be expressed using three rotation angles. The rotation angles of $O_L Y_L Z_L$ around three axes of $O_6 X_6 Y_6 Z_6$ can be considered as α, β and γ . Eq. (7) gives the detailed rotation matrix. Since Y_L and Z_L in $O_L Y_L Z_L$ corresponds to Y_6 and Z_6 in $O_6 X_6 Y_6 Z_6$, from Eqs. (2) and (7), a nonlinear equation set can be established in the form of Eq. (8). By solving this equation set, the rotation angle α, β and γ can be worked out, which reduces the number of the parameters in T_6^L from nine to six.

$$\begin{bmatrix} \cos\beta\cos\gamma & -\cos\beta\sin\gamma & \sin\beta \\ \sin\alpha\sin\beta\cos\gamma + \cos\alpha\sin\gamma & -\sin\alpha\sin\beta\sin\gamma + \cos\alpha\cos\gamma & -\sin\alpha\cos\beta \\ -\cos\alpha\sin\beta\cos\gamma & \cos\alpha\sin\beta\sin\gamma + \sin\alpha\cos\gamma & \cos\alpha\cos\beta \end{bmatrix}, \quad (7)$$

obtained in Figure 3 is not perfectly accurate. This is because that the scanning of the sphere is a handheld operation, and it would be difficult to manually maintain the constancy of both scanning speed and sensor orientation. On the other hand, since the sampling of the lines on the sphere is not continuous, the ground truth circle line corresponding to the biggest radius may not be captured. These inaccuracies in fixed-point measurements could cause errors in obtained conjugate pairs, thereby leading to errors in resultant T_6^L .

5 Searching the Optimal Solution of T_6^L

In Figure 3(b), the center of the circle with biggest radius corresponds to the center of the sphere. However, as mentioned in Section 4, it is difficult to get the circle that exactly passes through the center of the ball, which suggests that the T_6^L obtained might not be an exact solution.

To find the accurate result of T_6^L , a searching optimization approach is proposed. Firstly, the form of T_6^L is changed by reducing number of parameters in order to improve the efficiency of the search algorithm. In principle, the direction vectors (l_y, m_y, n_y) and (l_z, m_z, n_z)

$$\begin{cases} l_y = -\cos\beta\sin\gamma, \\ m_y = -\sin\alpha\sin\beta\sin\gamma + \cos\alpha\cos\gamma, \\ n_y = \cos\alpha\sin\beta\sin\gamma + \sin\alpha\cos\gamma, \\ l_z = \sin\beta, \\ m_z = -\sin\alpha\cos\beta, \\ n_z = \cos\alpha\cos\beta. \end{cases} \quad (8)$$

As shown in Figure 5, the parameters t_x, t_y, t_z solved in Section 4 and α, β, γ solved from Eq. (8) are taken as initial values. The search process is to find the optimal results $opt_t_x, opt_t_y, opt_t_z, opt_alpha, opt_beta$ and opt_gamma from $-range$ to $+range$. As long as the range setting is reasonable, the optimal value must be within this range. The green dot in the figure are the optimal results.

The search process is implemented through six-layer loops:

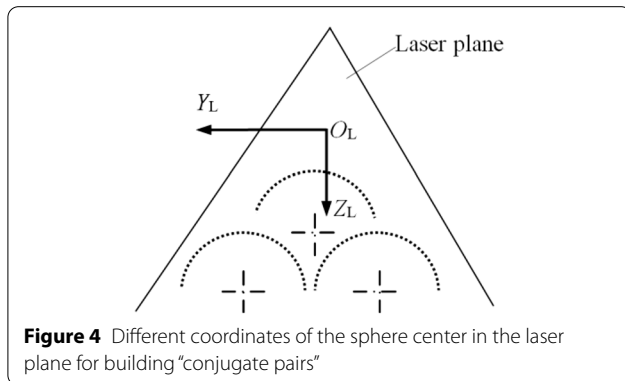


Figure 4 Different coordinates of the sphere center in the laser plane for building “conjugate pairs”

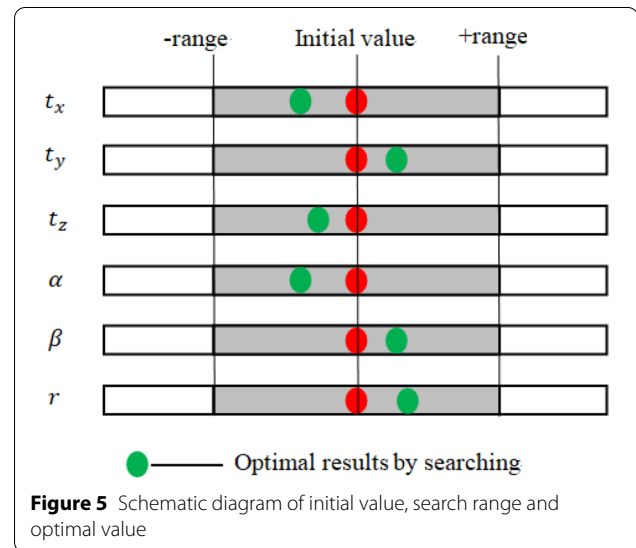


Figure 5 Schematic diagram of initial value, search range and optimal value

```

Smin=MAXVALUE
FOR(l=-times; l<= times; l++)
{
  tx = txref + lΔtx
  FOR(m= - times; m<= times; m++)
  {
    ty = tyref + mΔty
    FOR(n=- times; n<= times; n++)
    {
      tz = tzref + nΔtz
      FOR(i= - times; i<= times; i++)
      {
        α = αref + iΔα
        FOR(j= - times; j<= times; j++)
        {
          β = βref + jΔβ
          FOR(k=- times; k<= times; k++)
          {
            γ = γref + kΔγ
            S=Sph_fit(tx, ty, tz, α, β, γ)
            IF(S<Smin)
            {
              Smin=S
              opt_tx=tx
              opt_ty=ty
              opt_tz=tz
              opt_α=α
              opt_β=β
              opt_γ=γ
            }
          }
        }
      }
    }
  }
}

```

Where t_{xref} , t_{yref} , t_{zref} , α_{ref} , β_{ref} , γ_{ref} are the initial value of t_x , t_y , t_z , α , β , γ . Each parameter is changed from the corresponding initial value by small steps Δt_x , Δt_y , Δt_z , $\Delta \alpha$, $\Delta \beta$, $\Delta \gamma$ in the six loops. All points on the circle lines captured for calibration are used to fit a sphere. Sph_fit(t_x , t_y , t_z , α , β , γ) is the function which transforms the 2D data points in $O_L Y_L Z_L$ into 3D data points in $O_0 X_0 Y_0 Z_0$ using a group of ($t_x, t_y, t_z, \alpha, \beta, \gamma$), fits sphere using the 3D data points, and computes the distance between each 3D point to the fitted surface. S is the sum of the distance between each 3D point and the fitted surface and S_{min} is the smallest value of S . The parameters corresponding to S_{min} are opt_t_x , opt_t_y , opt_t_z , $opt_α$, $opt_β$ and $opt_γ$, which are searched optimal parameters.

In order to reduce the total search time, the search algorithm were executed several times in a coarse-to-fine manner. Firstly, the search algorithm is performed with a larger step size to find a set of optimal values. Then, by taking the optimal values as new initial values, a finer search algorithm is carried out using smaller steps. In Section 6.1, four rounds of search optimizations were performed. As shown in Table 1, in each search process, the cycles number corresponding to each variable is 11, that is, from -5 to $+5$. The searching steps of t_x , t_y , t_z gradually decreases from 0.625 to 0.005, while the search steps of α , β , γ gradually changes from 0.125° to 0.001°.

Table 1 Steps of the six parameters in the searching algorithm

	$\Delta t_x, \Delta t_y, \Delta t_z$ (mm)	$\Delta \alpha, \Delta \beta, \Delta \gamma$ (°)
First time	0.625	0.125
Second time	0.125	0.025
Third time	0.025	0.005
Fourth time	0.005	0.001

In this study, 40 lines are obtained on the sphere, and the number of points on each line is about 25, so the total number of points on the sphere is about 1000. The number of cycles corresponding to each variable is 11. Using i7-CPU for search operation, the time of one search is about 20 s, and the total time of four searches is 80 s.

6 Experimental Studies

6.1 Calibration Result

The AACMM adopted in this paper is Romer 2028, with the working diameter 2800 mm, repeatability 0.025 mm (3 σ), and length accuracy 0.066 mm (3 σ). The laser line sensor is self-made with the working depth 80 mm, and line length 65 mm. The repeatability is 0.008 mm, the measuring accuracy is 0.045 mm, and the standard working distance is 90 mm.

According to the proposed calibration method, 40 lines on the sphere are captured from different directions. Using obtained 40 conjugate pairs, the parameters in Eq. (2) are computed as:

$$\begin{bmatrix} l_y & l_z & t_x \\ m_y & m_z & t_y \\ n_y & n_z & t_z \\ 0 & 0 & 1 \end{bmatrix} = \begin{bmatrix} -0.997642 & 0.0314107 & 1.079 \\ 0.0596228 & -0.043697 & -3.465 \\ -0.033985 & -0.998555 & -211.168 \\ 0 & 0 & 1 \end{bmatrix} \quad (9)$$

The 2D data points on 40 measured lines are then transformed into 3D data points by substituting Eq. (9) into Eq. (4), and the 3D data points are employed to fit a sphere. Figure 6 demonstrates the distance between each point and the fitted surface. The biggest distance from the points outside the sphere and inside the sphere to the fitted surface are 0.483 mm and 0.576 mm, respectively.

To improve the accuracy of the parameters in T_6^L , the searching algorithm was executed four times. The cycle index of each loop is always fixed at 11, while the incremental steps for each time are listed in Table 1.

The optimized result of current iteration will be taken as a reference value for the next iteration. The final optimized parameters are

$$\begin{bmatrix} l_y & l_z & t_x \\ m_y & m_z & t_y \\ n_y & n_z & t_z \\ 0 & 0 & 1 \end{bmatrix} = \begin{bmatrix} -0.997193 & 0.0348994 & 1.465 \\ 0.0644936 & -0.048820 & -3.170 \\ -0.038018 & -0.998197 & -211.604 \\ 0 & 0 & 1 \end{bmatrix} \quad (10)$$

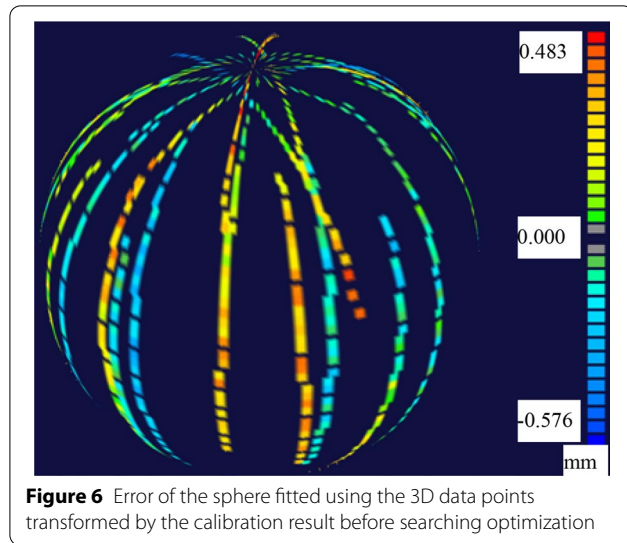


Figure 6 Error of the sphere fitted using the 3D data points transformed by the calibration result before searching optimization

The 2D data points on the 40 lines are also transformed into 3D data points by substituting Eq. (10) into Eq. (4), and the 3D data points are employed to fit a sphere. In Figure 7, the biggest distance from the point outside the sphere and inside the sphere to the fitted surface are 0.175 mm and 0.142 mm, respectively. It can be noticed that the accuracy the parameters in T_6^L is greatly improved after the searching optimization.

6.2 Error Analysis

The spatial accuracy of the AACMM is 0.066 mm (3σ), and the accuracy of the laser line sensor is 0.045 mm, which is usually considered as the error of a single scanned point. In this study, we test this error on a Hexagon bridge CMM. After the sensor is mounted on the

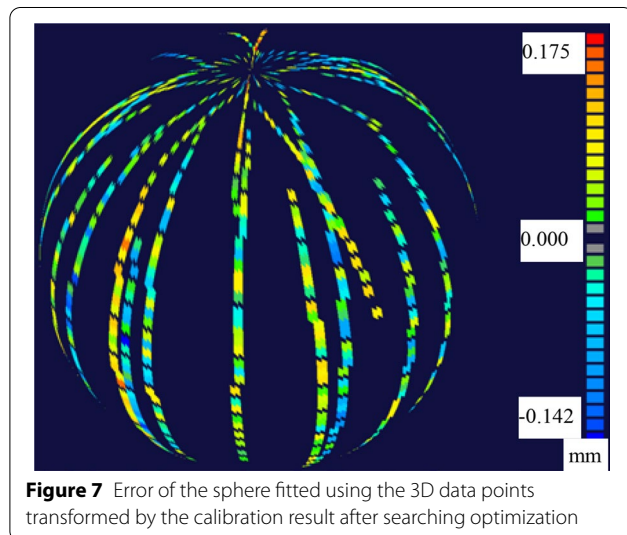


Figure 7 Error of the sphere fitted using the 3D data points transformed by the calibration result after searching optimization

CMM, the extrinsic parameters are calibrated. A sphere with the nominal radius 19.875 mm is scanned using the sensor. The scanned 3D data points are then applied to fit sphere with a fitted radius at 19.870 mm. The error between the nominal radius and the fitted radius is 0.005 mm, and the fitted radius is the result of all scanning point operations. We define this error as the systematic error of the sensor. While the biggest distance from the 3D points to the fitted sphere surface is 0.045 mm, it is regarded as the random error of the sensor.

The error of the AACMM and the laser sensor can cause errors in the process of calibration. Even if a fixed point is exactly measured, the errors in T_0^6 and (y_L, z_L) can also cause errors in T_6^L . Since (y_L, z_L) is achieved by circle fitting, the error of (y_L, z_L) is much smaller than the sensor error, which suggests that the error of the AACMM is the main error source of calibration error. In summary, there exist four types of errors in this system, which are defined as follows:

err_A : Error of the AACMM,

err_{SS} : The systematic error of the laser sensor,

err_{SR} : Random error of the laser sensor,

err_C : Calibration error of the system.

The maximum total error of the system is

$$\begin{aligned} err_{Total} &= err_A + err_{SS} + err_{SR} + err_C \\ &= 0.066 + 0.005 + 0.045 + err_C. \end{aligned} \quad (11)$$

Since the magnitude of err_C is unknown, err_{Total} cannot be directly calculated.

6.3 Accuracy Test

The measuring accuracy of the system is tested by scanning a plate and a reference sphere. The plate was scanned five times from different directions. For each scanning, only one or two joints of the AACMM were rotated, while other joints were kept fixed as far as possible. Firstly, the points on each scanned data patch are used to fit a plane, and the biggest distance from the points on each data patch to the corresponding fitted plane is defined as D_{pp_i} ($i = 1, 2, 3, 4, 5$), listed in Table 2. Then, the points on all five data patches are together

Table 2 Biggest distance from the points on each data patch to the fitted plane

Patches	$D_{pp_i}(\text{mm})$
patch 1	0.121
patch 2	0.132
patch 3	0.147
patch 4	0.116
patch 5	0.138

utilized to fit a plane, and the biggest distance from the points on five data patches to the fitted plane is 0.193 mm.

The measurement error mainly depends on the error of the arm and the sensor, and the error of arm comes from the position errors of the six axes. When scanning the plate from one direction, only one or two joints of the AACMM were rotated with other joints kept fixed. Thus, the biggest distance from the points to the fitted plane is majorly affected by the error of the one or two joints and the sensor. On the other hand, the position error of the entire data patch is mainly caused by the position errors of other axes. If all five data patches are applied to fit a plane, the fitted error could be attributed to the position errors of the six axes and the sensor. As a result, fitted error of five data patches (around 0.193 mm) is significantly greater than errors in single data patch D_{PPi} .

The sphere was also scanned from five directions. At each direction, only one or two joints of the AACMM were rotated. The points on the edge of each data patch have greater errors, thereby removed from the data patch using the software Surfer V10.0. Five spheres were fitted using the remaining points on each data patch, defined as SPH_i ($i = 1, 2, 3, 4, 5$). In Table 3, R_i represents the fitted radius, and D_{PSi} ($i = 1, 2, 3, 4, 5$) gives the biggest distance from the points on each data patch to the corresponding fitted sphere. Then the points on five data patches are utilized to fit a sphere, defined as SPH_{ALL} . The biggest distance from the points to the fitted sphere is 0.219 mm, which is greater than D_{PSi} in Table 3. The distances between the center of SPH_{ALL} and the centers of SPH_i are also given in Table 3.

It can be seen from the above test:

- (1) According to Eq. (11), total errors of the system are 0.193 mm and 0.219 mm, corresponding to scanning a plate and a sphere from five directions, respectively.
- (2) In Table 3, $|SPH_{ALL} - SPH_i|$ can represent the error between two data patches. Apparently, this error is

caused by the position errors of different joints of the AACMM. Hence, err_A is its main error source.

- (3) The R_i in Table 3 is close to the nominal radius of the sphere, since R_i is the radius of the fitted sphere by the data scanned from one direction. In this case, err_A is much smaller than 0.066 mm, and err_{SR} is greatly reduced after sphere fitting. Therefore, err_C and err_{SS} are the main error sources in R_i .

Typically, when measuring a complicated part, all joints are required to be rotated. In the above test, the total error of measuring a sphere is 0.219 mm. This error can be regarded as the measuring error of this system, since when scanning the sphere from five directions, all of the joints of the AACMM are rotated.

It can be found that the error of the AACMM is the main error source. It is worth noting that the calibration error is also an error source, but its magnitude cannot be found out.

7 Applications

To test the performance of this system, a model shown in Figure 8 is designed and manufactured with complex features of spheres, hole, square holes, and quadrangulars. Complete scanning of concave and convex semispheres can be achieved relatively easily. The four quadrangulars and the cylinder can be also completely measured from many directions. For circular and square holes, only the areas around the upper inside surface are scanned, as the deep areas cannot be accessed even though all the arms are rotated to try to find a suitable sensor orientation. Figure 9 shows the shaded form of the scanned data processed in Geomagic Studio 12. In this figure, there is no data on the deep area of the circular hole and the bottom of the square holes. As described in Section 1, the

Table 3 Biggest distance from the points on each data patch to the fitted sphere (mm)

Patches	R_i	$ SPH_{ALL} - SPH_i $	D_{PSi}
Patch 1	19.877	0.012	0.145
Patch 2	19.870	0.025	0.163
Patch 3	19.882	0.022	0.139
Patch 4	19.874	0.038	0.127
Patch 5	19.866	0.026	0.144

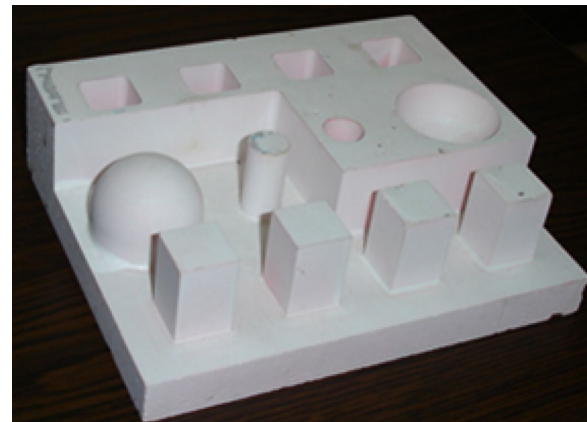


Figure 8 Picture of the model with specially fabricated complex features

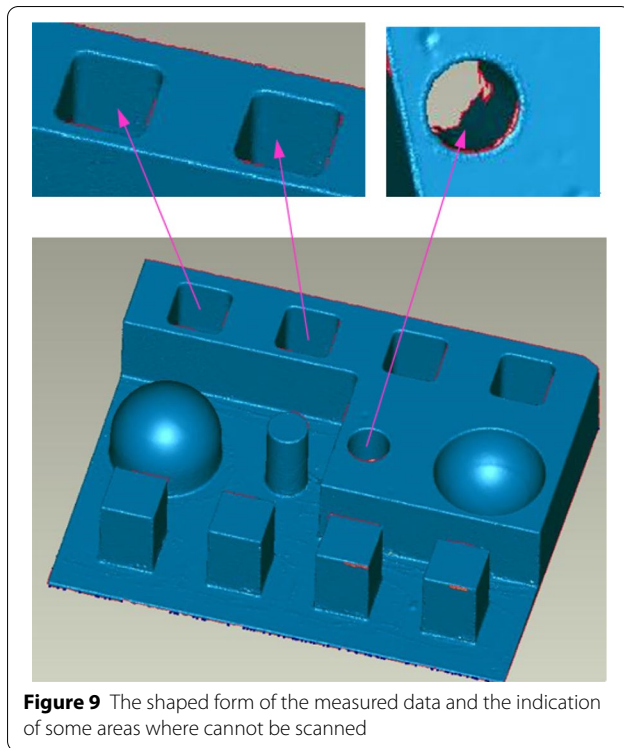


Figure 9 The shaped form of the measured data and the indication of some areas where cannot be scanned

working principle of the sensor is based on triangulation method, which suggests that the projected light cannot be received by the CCD camera if there exists sheltering. In this test, when scanning the hole, it is the hole itself which shelters the reflected light. Therefore, in principle, the sensor cannot scan the deep area of a hole, even though the AACMM provides adequate flexibility to the sensor. To sum up, most features of the model are completely measured using the system. This indicates that the system is flexible and facilitate to measure a part from any necessary direction.

8 Conclusions

This paper presents a flexible scanning method by integrating laser line sensors with articulated arm coordinate measuring machines. For a commercial articulated arm CMM, the transformation from the touch probe coordinate frame to the AACMM base coordinate frame can be directly accessed. By establishing the transformation from the 2D sensor coordinate frame into the sixth coordinate frame, the 2D data can be transformed into 3D data in the AACMM base coordinate frame. In order to solve the transformation model, “conjugate pairs” are introduced and determined by fixing the scanned points. In this study, a sphere is scanned with the data points fitted to a circle. The particular circle with a biggest radius is then used to locate the laser plane that passes through

the sphere center. To improve the accuracy of the transformation model, a searching approach is proposed to find the optimal solution. Experimental studies revealed that the measurement error is about 0.2 mm, which consist of the error of the AACMM, the sensor error, and the calibration error. The error of the AACMM is identified to be the main error source of the system, which leads to errors in conjugate pairs during calibration, as well as measurement errors during scanning. Its value varies with the number of the rotated axes, i.e., increasing the number of rotation axes could result in a greater error of the AACMM.

Therefore, when scanning an area of a part, the AACMM should be smoothly moved by rotating one or two arms. When the viewpoint of the sensor is not suitable for scanning, the orientation of the sensor should be changed by rotating other axes of the AACMM.

Acknowledgements

Not applicable.

Authors' Contributions

ZX proposed the calibration method; PY and HG wrote the manuscript; SC was in charge of the whole trial; XG assisted with sampling and laboratory analyses. All authors read and approved the final manuscript.

Authors' Information

Zexiao Xie, born in 1968, is currently an professor at *College of Engineering, Ocean University of China*. He received his PhD degree from *Tianjin University, China*, in 2000. His research interests include machine vision and robotics, underwater three-dimensional detection technology. Tel: +86-532-66781109; E-mail: xiezexiao@ouc.edu.cn

Ping Yu, born in 1995, is currently a master candidate at *College of Engineering, Ocean University of China*. E-mail: yuping_ouc@126.com

Hanlei Gong, born in 1996, is currently a master candidate at *College of Engineering, Ocean University of China*. E-mail: 1799217669@qq.com

Shukai Chi, born in 1980, is currently a senior engineer at *College of Engineering, Ocean University of China*. He received his PhD degree from *Ocean University of China*, in 2016. E-mail: chishukai@163.com

Xiang Gao, born in 1990, is currently a lecturer at *College of Engineering, Ocean University of China*. He received his PhD degree from *Institute of Automation, Chinese Academy of Sciences, China*, in 2019. E-mail: xgao@ouc.edu.cn

Funding

Supported by National Natural Science Foundation of China (Grant No. 42076192).

Competing interests

The authors declare no competing financial interests.

Received: 30 June 2020 Revised: 4 April 2022 Accepted: 6 July 2022

Published online: 06 September 2022

References

- [1] T Segreto, A Bottillo, R Teti. Non-contact reverse engineering modeling for additive manufacturing of down scaled cultural artefacts. *Procedia CIRP*, 2017, 62: 481–486.
- [2] K Kawazoe, T Kubota, Y Deguchi. Development of receiver optics for simplified 3D laser scanner composition. *Measurement*, 2019, 133: 124–132.
- [3] J Liang, H D Zhao, F C Song. Development of a laser-based measuring system for the inner geometrical dimension of cylinder line. *Results in Optics*, 2020, 1: 1–8.

- [4] K J He, C Y Sui, T Y Huang. 3D Surface reconstruction of transparent objects using laser scanning with .LTFTF method. *Optics and Lasers in Engineering*, 2022, 148: 1–10.
- [5] M Javaid, A Haleem, R P Singh, et al. Industrial perspectives of 3D scanning: Features, roles and its analytical applications. *Sensors International*, 2021, 2: 1–11.
- [6] Y J Shen, X Zhang, Z Y Wang, et al. A robust and efficient calibration method for spot laser probe on CMM. *Measurement*, 2020, 154: 1–10.
- [7] X Huang, Z Liu, J Zhao. Surface detection method with line structured light in complex environment. *Optical Precision Engineering*, 2016, 24 (10): 682–689.
- [8] N Ravikumar, A Gooya, S Çimen, et al. Group-wise similarity registration of point sets using Student's t-mixture model for statistical shape models. *Medical Image Analysis*, 2018, 44: 156–176.
- [9] M Guislain, J Digne, R Chainé, et al. Fine scale image registration in large-scale urban LIDAR point sets. *Computer Vision and Image Understanding*, 2017, 157: 90–102.
- [10] J H Sun, D L Ding, X Q Cheng, et al. Calibration of line-structured light vision sensor based on free-placed single cylindrical target. *Optics and Lasers in Engineering*, 2022, 152: 1–7.
- [11] Z L Zhou, W Liu, Y X Wang, et al. A combined calibration method of a mobile robotic measurement system for large-sized components. *Measurement*, 2022, 189: 1–16.
- [12] Y Li, Y J Fu, K J Zhong, et al. A virtual binocular line-structured light measurement method based on a plane mirror. *Optics Communications*, 2022, 510: 1–8.
- [13] S Zhang. Flexible and high-accuracy method for uni-directional structured light system calibration. *Optics and Lasers in Engineering*, 2021, 143: 1–5.
- [14] X B Xu, Z W Fei, J Yang, et al. Line structured light calibration method and centerline extraction: A review. *Results in Physics*, 2020, 19: 1–17.
- [15] Y H Li, B C Zhao, J B Zhou, et al. A universal method for the calibration of swing-scanning line structured light measurement system. *Optik*, 2021, 241: 1–10.
- [16] Z Z Wei, L J Cao, G J Zhang. A novel 1D target-based calibration method with unknown orientation for structured light vision sensor. *Optics & Laser Technology*, 2010, 42: 570–574.
- [17] Z Y Shi, T Wang, J C Lin. A simultaneous calibration technique of the extrinsic and turntable for structured-light-sensor-integrated CNC system. *Optics and Lasers in Engineering*, 2021, 138: 1–11.
- [18] Z X Xie, C G Zhang, Q M Zhang. A simplified method for the extrinsic calibration of structured-light sensors using a single-ball target. *International Journal of Machine Tools and Manufacture*, 2004, 44(11): 1197–1203.
- [19] J Santolaria, J J Pastor, F J Brosed, et al. A one-step intrinsic and extrinsic calibration method for laser line scanner operation in coordinate measuring machines. *Measurement Science and Technology*, 2009, 20(4): 1–12.
- [20] Z X Xie, X M Wang X, S K Chi. Simultaneous calibration of the intrinsic and extrinsic parameters of structured-light sensors. *Optics and Lasers in Engineering*, 2014, 58: 9–18.
- [21] H Du, X Chen, J Xi, et al. Development and verification of a novel robot-integrated fringe projection 3D scanning system for large-scale metrology. *Sensors*, 2017, 17 (12): 2886.
- [22] X J Pan, J Y Wu, Z L Li, et al. Self-calibration for linear structured light 3D measurement system based on quantum genetic algorithm and feature matching. *Optik*, 2020, 255: 1–10.
- [23] J D Han, W F Lv, F Wang. 3D data registration method based on optical location tracking technology. *Optical Precision Engineering*, 2009, 17(1): 45–51.
- [24] J Chen, X J Wu, Y Wang, et al. 3D shape modeling using a self-developed hand-held 3D laser scanner and an efficient HT-ICP point cloud registration algorithm. *Optics & Laser Technology*, 2013, 45: 414–423.
- [25] S Yin, Y Ren, Y Guo, et al. Development and calibration of an integrated 3D scanning system for high-accuracy large-scale metrology. *Measurement*, 2014, 54(8): 65–76.
- [26] S Sharifzadeh, I Biro, P Kinnell. Robust hand-eye calibration of 2D laser sensors using a single-plane calibration artefact. *Robotics and Computer-Integrated Manufacturing*, 2020, 61: 1–10.
- [27] Y Qin, R K Kang, J S Sun. A fast self-calibration method of line laser sensors for on-machine measurement of honeycomb cores. *Optics and Lasers in Engineering*, 2022, 152: 1–14.
- [28] H T Yu, Y Huang, D L Zheng. Three-dimensional shape measurement technique for large-scale objects based on line structured light combined with industrial robot. *Optik*, 2020, 202: 1–11.

Submit your manuscript to a SpringerOpen[®] journal and benefit from:

- Convenient online submission
- Rigorous peer review
- Open access: articles freely available online
- High visibility within the field
- Retaining the copyright to your article

Submit your next manuscript at ► [springeropen.com](https://www.springeropen.com)